Hindawi
Shock and Vibration
Volume 2024, Article ID 7755652, 13 pages
https://doi.org/10.1155/2024/7755652

Research Article

Burst Failure Characteristics and Energy Evolution Law of Coal with Prefabricated Cracks at Different Angles

Xiufeng Zhang,[1] Yueyong Han,[1] Yang Chen,[1] Xingyin Ma,[2] Xinrong Zhang,[1] Cao Man,[1] and Yanchun Yin[2]

[1]*Shandong Energy Group Co., Ltd., Jinan 250101, China*
[2]*College of Energy and Mining Engineering, Shandong University of Science and Technology, Qingdao 266590, China*

Correspondence should be addressed to Xingyin Ma; 1365796096@qq.com

Received 2 November 2023; Revised 18 January 2024; Accepted 8 February 2024; Published 15 March 2024

Academic Editor: Lei Weng

In order to study the influence of fissures on the burst tendency of coal, the test and numerical simulation of the burst tendency of coal with different burst angles were carried out. The evolution law of the burst tendency index of coal under the influence of burst angle was analyzed, and the mechanism of energy storage and release of coal under the influence of fissure angle was revealed. The results show that compared with the specimens without prefabricated cracks, the uniaxial compressive strength of the specimens with 0° cracks is reduced by 48.4%, the dynamic failure time is increased by 279.4%, the burst energy index is reduced by 54%, and the burst energy velocity index is reduced by 87.9%. After that, with the increase of prefabricated crack angle, the uniaxial compressive strength of coal increases gradually, the dynamic failure time decreases gradually, the burst energy index increases gradually, and the burst energy velocity index increases gradually. That is to say, the larger the crack angle contained in the coal body, the stronger the burst tendency of the coal body, but it is still lower than that of the complete coal body. With the increase of prefabricated crack angle, the proportion of prepeak elastic energy of coal body increases, the less energy dissipation in the whole loading process of coal body, and the faster energy release rate during failure. The research results can provide some theoretical support for the prevention and control of rock burst disaster.

1. Introduction

Coal is a typical heterogeneous material that contains a large number of joints, cracks, or structural planes inside. The instability and failure of coal mine roadways are caused by the initiation, expansion, and connection of internal cracks in the coal body [1–4]. With the gradual deepening of coal mining, the joint cracks of the roadway surrounding rock are more developed, loose, and broken, and the deformation of the roadway is aggravated [5–9]. The fracture of coal can be regarded as a process of energy conversion and transmission, and its final failure is a state instability phenomenon driven by energy. Many scholars believe that the essential mechanism of coal dynamic failure and rock burst can be revealed from the perspective of energy [10–14]. Therefore, it is of great engineering significance to study the burst failure and energy evolution of cracked coal.

At present, scholars at home and abroad have systematically studied the influence of crack dip angle, number and length on the strength, and deformation and failure characteristics of coal mass through laboratory tests and numerical simulation [15–19].

The whole process from loading deformation to destruction of coal body is accompanied by the accumulation and transformation of energy. Energy is the essential factor leading to the destruction of the coal bodies [19–26]. Many scholars have carried out a lot of research on energy and rock failure, but there are few studies on the energy of cracked coal, which still needs further research.

Previous studies have focused on the influence of crack angle, crack number, and crack length on the mechanical properties of coal and rock mass. Therefore, on the basis of previous studies, this paper fixed the crack length and crack number, prefabricated four kinds of coal with different crack

angles, and carried out the impact tendency test of coal with different crack angles to study the impact failure characteristics of coal [27, 28]. Through the indoor test and numerical simulation of coal body with different fracture angles, the energy evolution process of coal body is analyzed and the energy evolution law of coal body is studied.

2. Indoor Experiment and Result Analysis

2.1. Specimen Preparation and Loading Scheme. The size of the coal in the test is 50 mm in diameter and 100 mm in height. The prefabricated crack is located in the center of the coal body. The crack size is 20 mm in length and 2 mm in width, and the crack penetrates the coal body. In order to reduce the individual difference of the sample, the longitudinal wave velocity of the coal sample was tested before the prefabricated crack, and the coal sample with the wave velocity between 1200 and 1500 m/s was selected for the prefabricated crack. According to the angle of the prefabricated crack, it is divided into five groups of tests, namely, no crack group, 0° crack group, 30° crack group, 60° crack group, and 90° crack group. Each group is tested on three specimens. The specific specimen preparation is shown in Figure 1.

The test loading system adopts an RLJW-2000 rock testing machine, axial compression is applied at a stress loading rate of 0.5 mm/min, and the load-displacement data of the sample are collected synchronously until the sample is destroyed.

2.2. Measurement of Burst Tendency. The burst tendency of coal refers to the ability and inherent properties of coal to accumulate energy and produce burst damage, which is a necessary condition for rock burst. Therefore, the determination of coal burst tendency is an important part of the prevention and control of rock burst, and the burst tendency index can be used to evaluate the risk of coal burst. In the national standard GB/T 25217.2-2010 determination of rock burst monitoring and prevention methods Part 2: classification of coal burst tendency and determination method of index, four indexes are given to measure the strength of burst tendency. At the same time, many researchers have also proposed many indexes to measure the burst tendency [29, 30].

In this test, four parameters in the national standard, namely, dynamic failure time D_T, uniaxial compressive strength σ_c, burst energy index K_E, and burst energy velocity index W_{ST} proposed by authoritative scholars [28], were selected to measure the burst tendency of coal body, which can be divided into no burst tendency, weak burst tendency, and strong burst tendency.

The uniaxial compressive strength can reflect the ultimate bearing capacity of coal samples. The higher the uniaxial compressive strength, the stronger the bearing capacity of coal samples before failure, the more energy accumulated inside under the external force, and the greater the kinetic energy converted and released when the peak strength is reached. The dynamic failure time is used to measure the degree of burst tendency, which is the transient

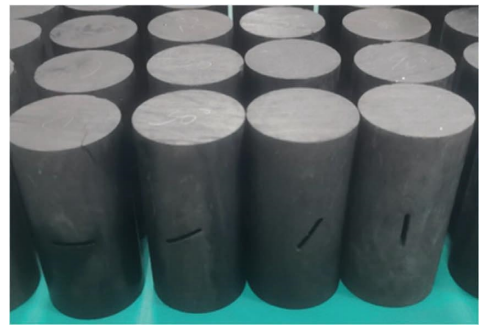

Figure 1: Coal specimens with prefabricated cracks at different angles.

duration time of coal from the beginning to the end of the peak strength, as shown in Figure 2 [29]. The duration of the failure process is a comprehensive reflection of the dynamic characteristics of energy accumulation and dissipation, reflecting the speed of postpeak failure of coal samples.

The whole process of the stress-strain curve of coal contains rich information about burst tendency, which intuitively and comprehensively reflects the whole process from energy storage to energy consumption. It is of great significance to reveal the physical nature of burst tendency and analyze other burst tendency indexes. The burst energy index is calculated by dividing the prepeak total input energy by the postpeak failure dissipation energy in the stress-strain curve, as shown in Figure 3 [29]. The calculation formula is as follows:

$$K_E = \frac{W_p}{W_f}. \tag{1}$$

In the formula, W_p is the total input energy before the peak, and its value is the area enclosed by the prepeak curve and the coordinate axis; W_f is the postpeak damage dissipation energy, and its value is the area enclosed by the postpeak curve and the coordinate axis.

The residual energy released per unit time during the failure process of coal samples represents the amount of elastic energy converted into kinetic energy per unit time, which also reflects the degree of burst tendency of coal. The burst energy velocity index is the ratio of the burst energy index to the dynamic failure time. The specific calculation formula is as follows:

$$W_{ST} = \frac{K_E}{D_T}. \tag{2}$$

The physical meaning of the index characterizes the ratio of energy accumulation and release during the compression process of coal samples per unit time and reflects the burst release ability of energy during the compression failure process of coal samples.

The determination methods of four burst tendency indexes are listed in Table 1.

2.3. The Final Failure Form of Coal. Figure 4 shows the final failure form of the coal specimen after uniaxial compression loading. It can be seen from Figure 4 that the damage degree

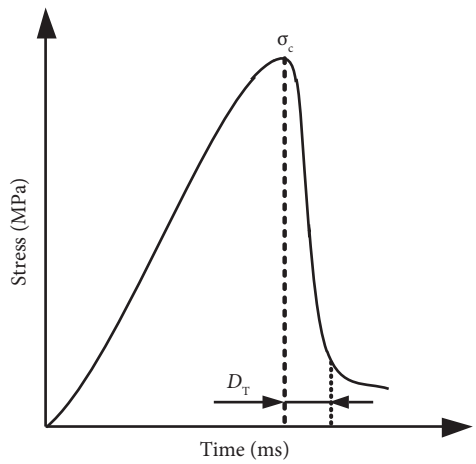

Figure 2: Dynamic failure D_T time calculation diagram [29].

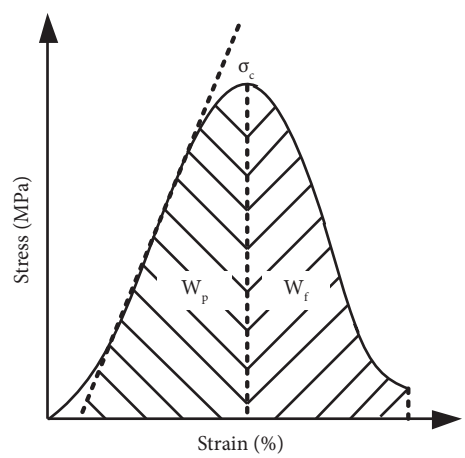

Figure 3: Burst energy index K_E calculation diagram [29].

of the 0° crack specimen is the smallest, and only a small number of fragments fall off along the crack tip. For the 30° crack specimen, some coal blocks are thrown along the crack area, and the whole crack area of the 60° crack specimen is basically completely destroyed, while the 90° crack specimen has large pieces of coal body spalling and throwing, and the degree of damage is the largest.

2.4. Uniaxial Compressive Strength σ_c. The stress-time curve of coal containing prefabricated cracks with different angles is shown in Figure 5. When the crack angle is 0°, 30°, and 60°, the postpeak curve is a step-down curve; the new cracks in the specimen are slowly generated and expanded, and the specimen is slowly destroyed. When the prefabricated crack angle increases to 90°, the step-down characteristic of the postpeak curve of the specimen weakens, showing rapid failure and enhanced brittle failure characteristics.

The statistics of uniaxial compressive strength of prefabricated cracks at different angles are shown in Table 2 and Figure 6. About the uniaxial compressive strength, compared with the specimens without prefabricated cracks, the uniaxial compressive strength of the coal is reduced by 48.4% when the crack angle is 0°, 44.9% when the crack angle is 30°, and 32.8% when the crack angle is 60°. The coal body with three crack angles shows a weak burst tendency; when the crack angle is 90°, the uniaxial compressive strength is reduced by 2%. In this case, it still shows a strong burst tendency. With the increase of prefabricated crack angle, the measured value of uniaxial compressive strength of coal specimens also increases, and a power function growth relationship is presented.

Since the coal is limited in the loading direction, there is free expansion space in the other two directions, so the microcracks are mainly tensile cracks parallel to the loading direction. In the mutual expansion and penetration of small tensile cracks, the prefabricated cracks play the role of bridging, so that the cracks generated inside the coal body with the increase of load can interact more easily, and then, the ability of the coal sample to withstand the load is reduced. Therefore, with the increase of the dip angle, the number of tensile cracks that can be connected by the prefabricated cracks of the same length along the loading direction is less and less, so the uniaxial compressive strength of the coal body is on the rise. Especially when the crack dip angle is 90°, the prefabricated crack has little effect on the uniaxial compressive strength of the coal body.

2.5. Dynamic Failure Time D_T. The dynamic failure time of coal obtained from the stress-time curve is shown in Table 3 and Figure 7. Compared with the coal specimen without prefabricated cracks, the dynamic failure time increases by 279.4% when the crack angle is 0°, 236.7% when the crack angle is 30°, 171.8% when the crack angle is 60°, and 15.9% when the crack angle is 90°. According to the standard, there is no burst tendency. With the increase of crack angle, the measured value of dynamic failure time gradually decreases and finally shows a trend of power function decrease. The smaller the crack angle, the longer the dynamic failure time of the specimen. This is because with the increase of the crack angle, the projection length of the crack length in the vertical loading direction is smaller, so that the number of cracks in the coal body parallel to the loading direction is reduced, the damage degree of the coal body is reduced, and finally, the dynamic failure time of the coal body is reduced.

2.6. Burst Energy Index K_E. Through the analysis of stress-strain curve data, the final calculated coal burst energy index is shown in Table 4 and Figure 8. Compared with the coal specimen without prefabricated cracks, the burst energy index is reduced by 54% when the crack angle is 0°, 42.2% when the crack angle is 30°, 24.4% when the crack angle is 60°, and 11.9% when the crack angle is 90°. As the crack angle increases, the measured value of the burst energy index gradually increases, showing a linear growth trend. The smaller the crack angle, the smaller the burst energy index of the coal, and the less severe the damage. The results also verify the influence principle of fracture angle on uniaxial compressive strength and dynamic failure time of coal.

Table 1: Determination of burst tendency [29, 30].

Burst tendency	No burst trend	Weak burst tendency	Strong burst tendency
Dynamic destruction time (ms)	>500	50~500	≤50
Uniaxial compressive strength (MPa)	<7	7~14	≥14
Bursting energy index	<1.5	1.5~5	≥5
Burst energy velocity index (s^{-1})	<3	3~100	≥100

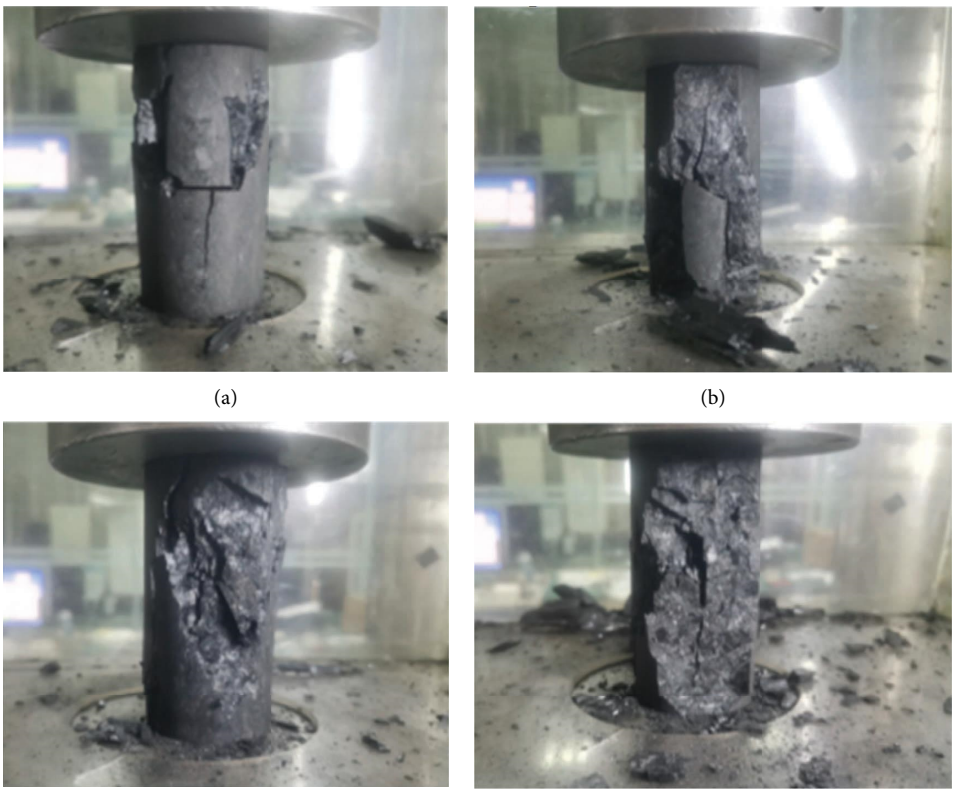

Figure 4: Final failure diagram under different crack angles: (a) 0°; (b) 30°; (c) 60°; (d) 90°.

2.7. Burst Energy Velocity Index W_{ST}. According to the average value of burst energy index and dynamic failure time and combined with formula (2), the final burst energy velocity index of coal is shown in Table 5 and Figure 9. According to the standard, the coal without prefabricated cracks has weak burst tendency. Compared with the coal without prefabricated cracks, the burst energy velocity index decreases by 87.9% when the crack angle is 0°, 82.6% when the crack angle is 30°, and 72.2% when the crack angle is 60°. The coal with these three abovementioned crack angles shows no burst tendency. When the crack angle is 90°, the burst energy velocity index is reduced by 23.9%, and this crack angle still shows a weak burst tendency. With the increase of crack angle, the measured value of burst energy velocity index increases gradually, showing a trend of power function growth. The smaller the crack angle, the smaller the burst energy velocity index of coal, and the less the elastic energy converted into kinetic energy per unit time.

3. Numerical Simulation and Result Analysis

3.1. Simulation Scheme. In order to study the energy evolution law of coal with prefabricated cracks at different angles, PFC numerical simulation software is used to establish a numerical model similar to the laboratory test. The model size is 50 mm × 100 mm, and the prefabricated crack angles are 0°, 15°, 30°, 45°, 60°, 75°, and 90°. The crack length is 20 mm, and the width is 2 mm. The crack is located at the center of the model.

In this simulation, the parallel bond model is used to simulate the mechanical behavior of coal. The parameters are compared by the trial and error method and indoor test. The stress-strain curve of the complete specimen is shown in Figure 10. The specific parameters of the model are listed in Table 6.

In PFC, rock crack and macroparameters are closely related to the size of particles, which is called the size effect. With increasing of L/R (i.e. the ratio of specimen size to

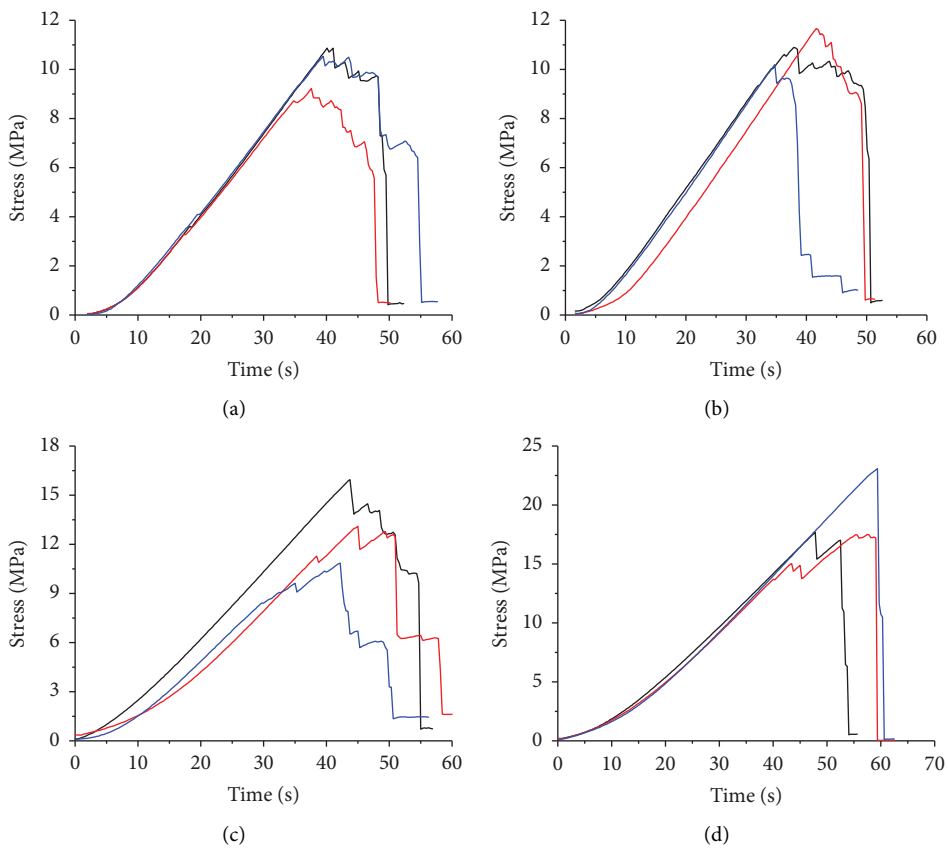

Figure 5: Stress-time curves under different crack angles: (a) 0°; (b) 30°; (c) 60°; (d) 90°.

Table 2: Uniaxial compressive strength of coal under different crack angles.

Specimen types	Group a (MPa)	Group b (MPa)	Group c (MPa)	Average value (MPa)
Complete cylinder	17.97	21.01	20.4	19.79
0° cracked cylinder	10.86	9.22	10.53	10.2
30° cracked cylinder	10.89	11.66	10.19	10.91
60° cracked cylinder	15.95	13.1	10.85	13.3
90° cracked cylinder	17.68	17.51	23.01	19.4

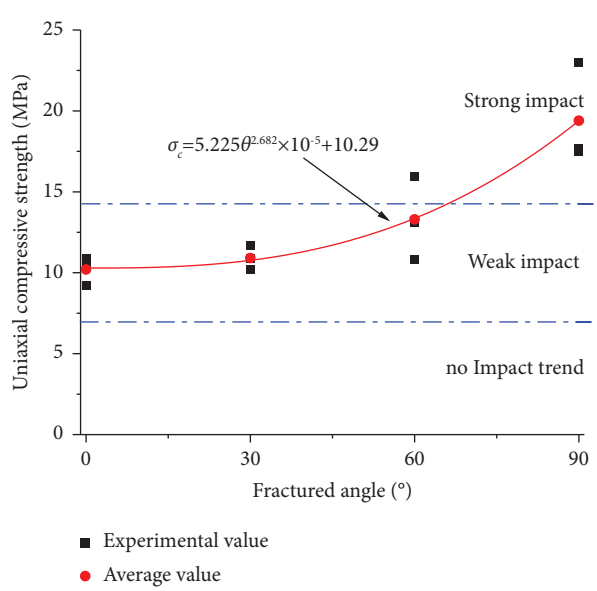

Figure 6: The relationship curve between crack angle and uniaxial compressive strength.

Table 3: Dynamic failure time of coal under different crack angles.

Specimen types	Group a (ms)	Group b (ms)	Group c (ms)	Average value (ms)
Complete cylinder	2500	1250	2183	1977
0° cracked cylinder	8438	7188	6875	7500
30° cracked cylinder	6562	6563	6845	6656
60° cracked cylinder	3750	6249	6120	5373
90° cracked cylinder	1563	3749	1563	2291

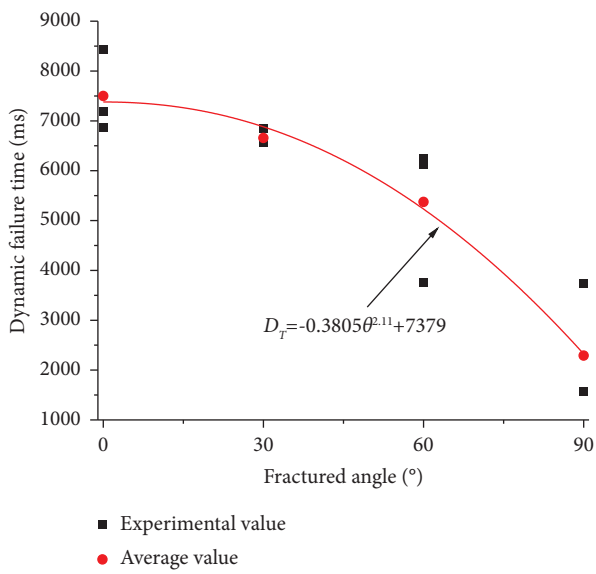

Figure 7: Relationship curve between crack angle and dynamic failure time.

Table 4: Bursting energy index of coal under different crack angles.

Specimen types	Group a	Group b	Group c	Average value
Complete cylinder	20.29	21.11	16.15	19.22
0° cracked cylinder	15.1	7.99	3.47	8.85
30° cracked cylinder	16.34	12.6	4.36	11.1
60° cracked cylinder	20.64	11.34	11.6	14.53
90° cracked cylinder	16.45	17.6	16.76	16.94

particle radius), the influence of the size effect decreases. Based on works by Zhao et al., when the value of L/R is greater than 120, the size of particles has little influence on macro parameters of the specimen [31]. So in this paper, in order to reduce the size effect, the radius of the particles was set 0.4~0.5 mm, and L/R was 220.

In the simulation, the coal is prefabricated with cracks at different angles, and then, uniaxial loading is carried out to destroy the coal. The changes of stress, elastic energy, dissipation energy, and input energy in the whole process are recorded, and the energy evolution law of the coal body is analyzed.

3.2. Failure Form of Specimen. After uniaxial loading to failure, the crack expansion of coal under different crack angles is shown in Figure 11. From the diagram, it can be seen that after uniaxial loading, the tip of the prefabricated crack will be destroyed first. With the increase of the angle of the prefabricated crack, the generated crack gradually expands to the diagonal direction. When the angle of the prefabricated crack is small, the damage range is basically near the prefabricated crack. The larger the angle of the prefabricated crack, the larger the damage range, which is basically similar to the indoor test results.

3.3. The Energy Calculation Method. In PFC2D simulation, the strain energy accumulated in the specimen includes two parts. One is the contact strain energy E_{str}^{c} stored at all contacts, and the other is the parallel-bond strain energy $E_{\text{str}}^{\text{pb}}$ stored in parallel bonds. The strain energy can be expressed as

$$E_{\text{str}} = E_{\text{str}}^{c} + E_{\text{str}}^{\text{pb}}, \tag{3}$$

where

$$E_{\text{str}}^{\text{pb}} = \frac{1}{2}\sum_{i\in N_{\text{pb}}}\left(\frac{\left|\overline{F}_i^n\right|^2}{A_i\overline{k}_i^n} + \frac{\left|\overline{F}_i^s\right|^2}{A_i\overline{k}_s^i} + \frac{\left|\overline{M}_i\right|^2}{I_i\overline{k}_n^i}\right), \tag{4}$$

$$E_{str}^{c} = \frac{1}{2}\sum_{i\in N_c}\left(\frac{\left|F_i^n\right|^2}{k_i^n} + \frac{\left|F_i^s\right|^2}{k_s^i}\right). \tag{5}$$

In Equations (4) and (5), $\overline{F}_i^n$, $\overline{F}_i^s$, and $\overline{M}_i^s$ are the normal force, shear force, and the moment in the parallel bond i, respectively; F_i^n and F_i^s are the normal force and shear force in the contact i, respectively; A_i and I_i are the area and inertia moment of the bond cross section, respectively; N_c is the number of contacts; and N_{pb} is the number of parallel bonds.

3.4. Energy Evolution Process of Coal with Different Crack Angles. During the loading process of the coal, the stress and energy evolution curve of the whole process can show the loading and failure process inside the coal during the whole process. The energy evolution law in the process of coal loading and failure is analyzed, respectively, as shown in Figure 12.

It can be seen from Figure 9 that as the prefabricated crack angle increases, the strain at failure gradually increases. When the prefabricated crack angle is 0°, the strain is 0.148%, and when it is 90°, the strain is 0.18%. The greater the angle of the prefabricated crack, the greater the uniaxial compressive strength and the greater the peak elastic energy; the larger the prefabricated crack angle is, the faster the release rate of stress and elastic energy in the postpeak failure stage is, the faster the dissipation energy increases, and the more severe the damage is.

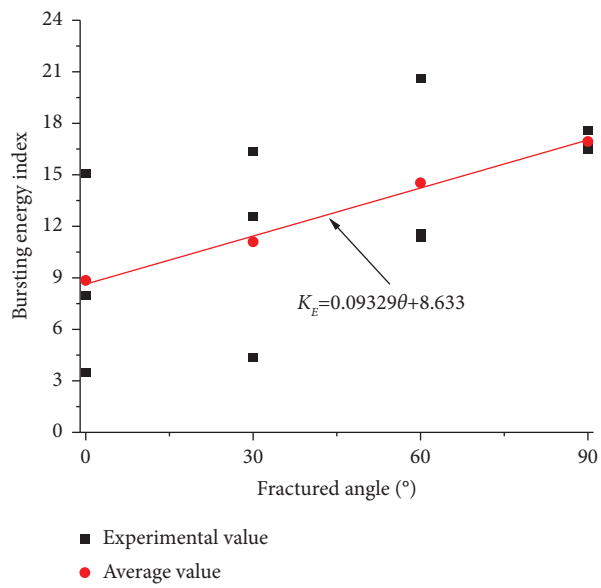

Figure 8: Relationship curve between crack angle and bursting energy index.

Table 5: Burst energy velocity index of coal under different crack angles.

Specimen types	Average value
Complete cylinder	19.22
0° cracked cylinder	8.85
30° cracked cylinder	11.1
60° cracked cylinder	14.53
90° cracked cylinder	16.94

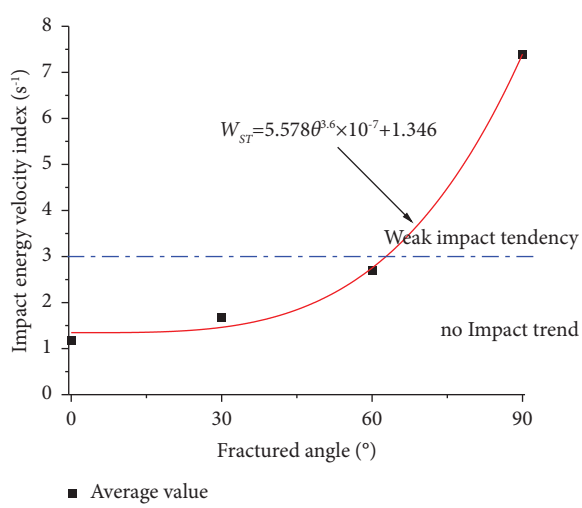

Figure 9: Relationship curve between crack angle and burst energy velocity index.

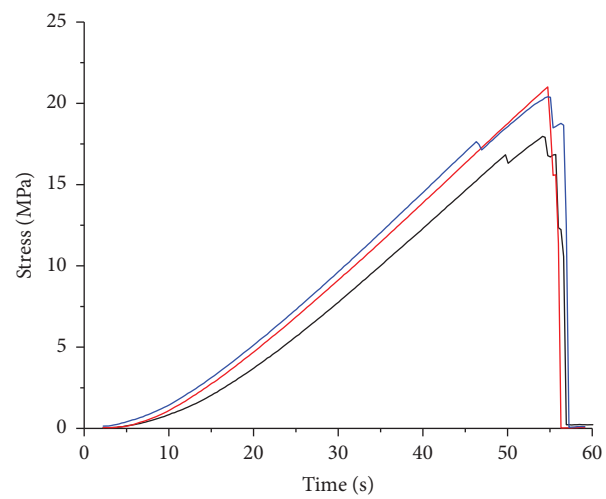

Figure 10: Stress-strain curve of complete specimen.

Table 6: Micromechanical parameters of coal samples.

Micromechanical parameters	Value
Minimum/maximum particle radius (mm)	0.004/0.005
Particle density (kg/m^3)	1700.0
Normal/tangential contact damping	0.7/0.5
Coefficient of friction	0.8
Parallel bond effective modulus (GPa)	1.7
Parallel bond normal strength (MPa)	14.0
Parallel bond tangential strength (MPa)	13.0

3.5. Energy Storage Law of Coal with Different Crack Angles. Compared with the noncracked coal, the uniaxial compressive strength and elastic energy peak of the cracked coal will change, resulting in the change of the maximum energy storage of the coal. Therefore, the uniaxial compressive strength and elastic energy peak of the nonprefabricated crack and different prefabricated crack angles are compared and analyzed.

Figure 13 shows the uniaxial compressive strength curve at different crack angles. The uniaxial compressive strength of coal without prefabricated cracks is 18.38 MPa. It decreases by 31.23% when the prefabricated crack angle is 0°,

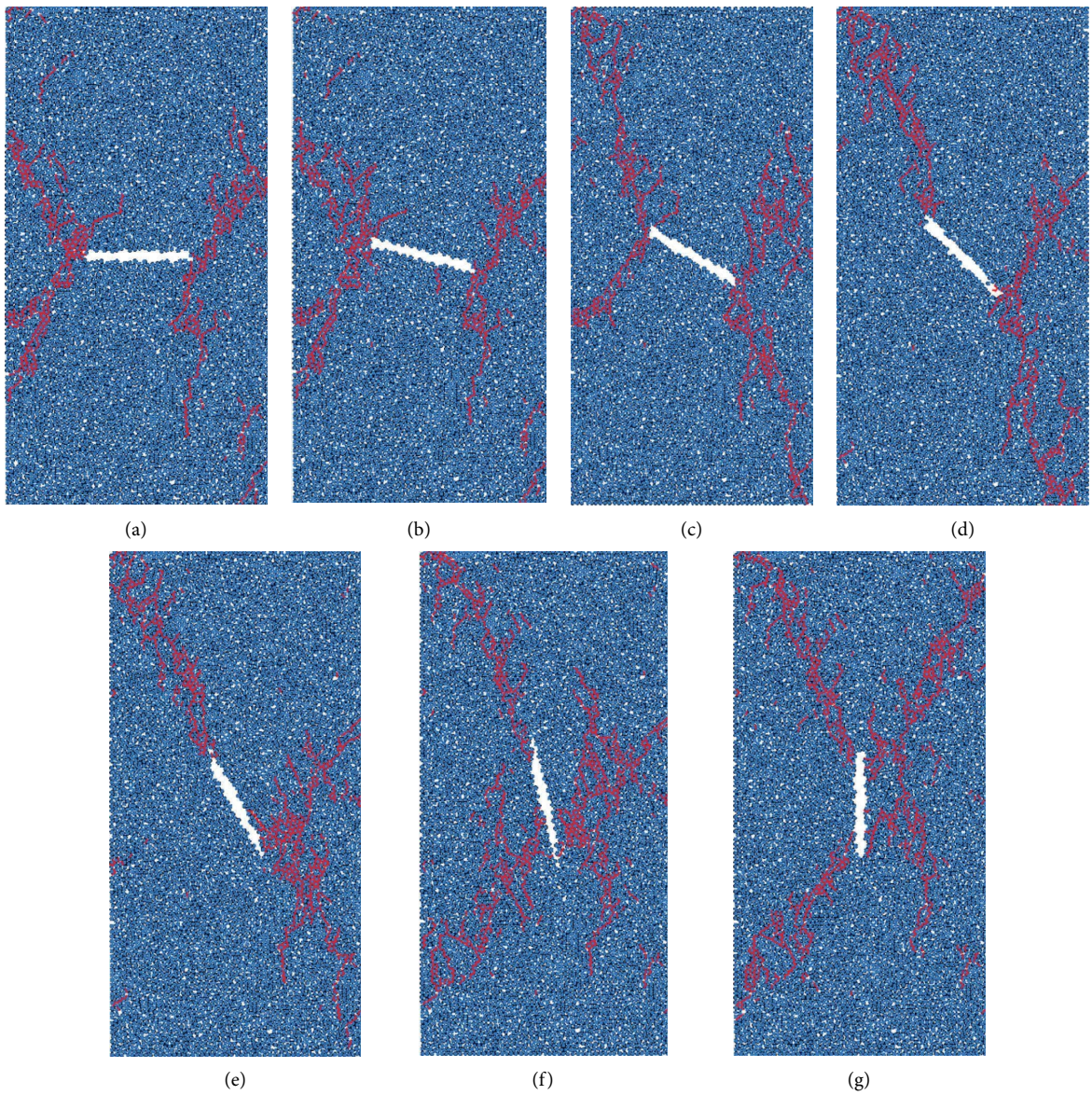

Figure 11: Coal fracture propagation under different crack angles: (a) 0° crack; (b) 15° crack; (c) 30° crack; (d) 45° crack; (e) 60° crack; (f) 75° crack; (g) 90° crack.

30.85% when the prefabricated crack angle is 15°, 25.79% when the prefabricated crack angle is 30°, 26.33% when the prefabricated crack angle is 45°, 16.81% when the prefabricated crack angle is 60°, 9.96% when the prefabricated crack angle is 75°, and 6.69% when the prefabricated crack angle is 90°. The greater the prefabricated crack angle of the coal body, the greater the uniaxial compressive strength increases in a power function, and the smaller the reduction is compared with the nonprefabricated crack, which is basically the same as the test results.

Figure 14 shows the peak curve of elastic energy at different crack angles. When there is no prefabricated crack, the peak value of elastic energy of coal is 93.67 J. It is reduced by 49.72% when the prefabricated crack angle is 0°, 47.91% when the prefabricated crack angle is 15°, 43.39% when the prefabricated crack angle is 30°, 45.5% when the prefabricated crack angle is 45°, 35.35% when the prefabricated crack angle is 60°, 27.15% at 75°, and 18.46% at 90°. The larger the prefabricated crack angle of the coal body, the peak value of the elastic energy increases in a power function, but it is still lower than the peak value of the elastic energy of the coal body without prefabricated cracks.

3.6. Energy Dissipation and Release Law of Coal with Different Crack Angles. During the whole loading process of the coal, there will be some energy dissipation. When the peak point is reached, the difference between the input energy and the elastic energy represents the energy dissipation during the whole loading process. Therefore, the elastic energy ratio (the ratio of the elastic energy peak to the input energy) is defined to analyze the energy dissipation law during the loading process of the coal.

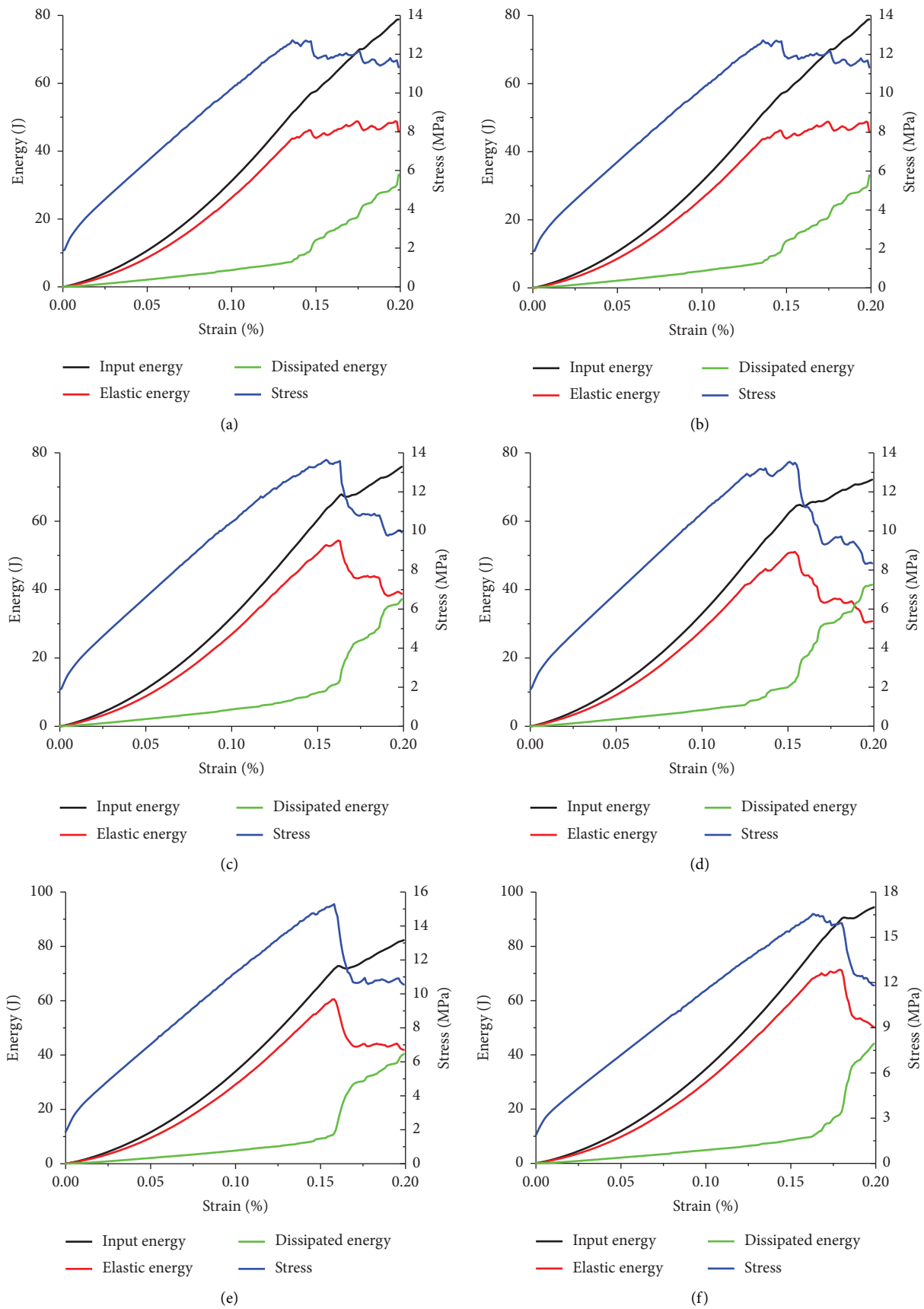

Figure 12: Continued.

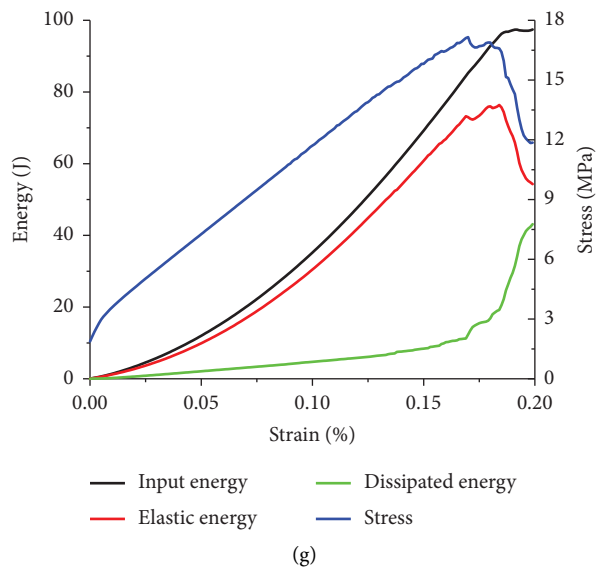

Figure 12: Energy evolution process of coal under different crack angles: (a) 0° crack; (b) 15° crack; (c) 30° crack; (d) 45° crack; (e) 60° crack; (f) 75° crack; (g) 90° crack.

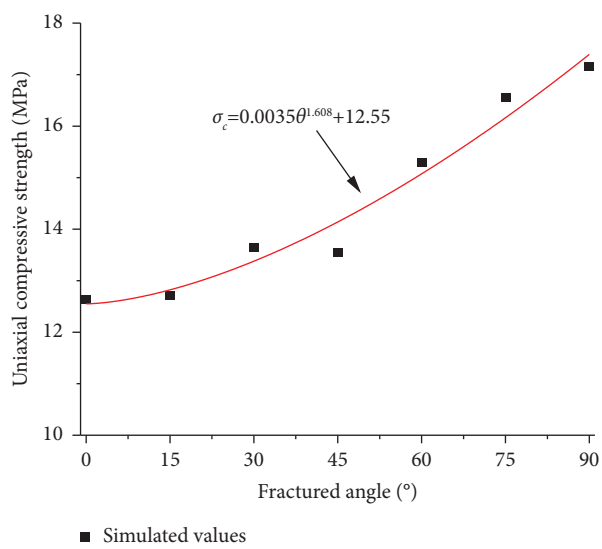

Figure 13: Uniaxial compressive strength curves at different crack angles.

Figure 15 shows the elastic energy ratio curve at different crack angles. When there is no prefabricated crack, the proportion of elastic energy of coal is 89.35%. It is reduced by 24.83% when the prefabricated crack angle is 0°, 18.75% when the prefabricated crack angle is 15°, 8.24% when the prefabricated crack angle is 30°, 9.68% when the prefabricated crack angle is 45°, 4.85% when the prefabricated crack angle is 60°, 2.18% at 75°, and 2.64% at 90°. The larger the prefabricated crack angle of coal body is, the larger the proportion of elastic energy is, showing a power function. Compared with no prefabricated crack, the smaller the reduction range is, the less the energy dissipation in the whole loading process of coal body is.

In the loading process of the whole coal body, the proportion of elastic energy can reflect the energy storage and dissipation characteristics inside the coal body. The postpeak energy release rate (i.e., failure energy release rate) can reflect the speed of energy release after coal failure. The slower the postpeak energy release rate is, the lower the burst risk of postpeak failure is. Figure 16 shows the energy release rate curves of coal with different crack angles after failure. For the postpeak failure stage, when the prefabricated crack angle is 0°, the elastic energy release amount of each 1% strain is 143.1 J, and the elastic energy release amount of each 1% strain increases by 8.04% at 15°. At 30°, the elastic energy release amount of each 1% strain increases by 126.62%. At

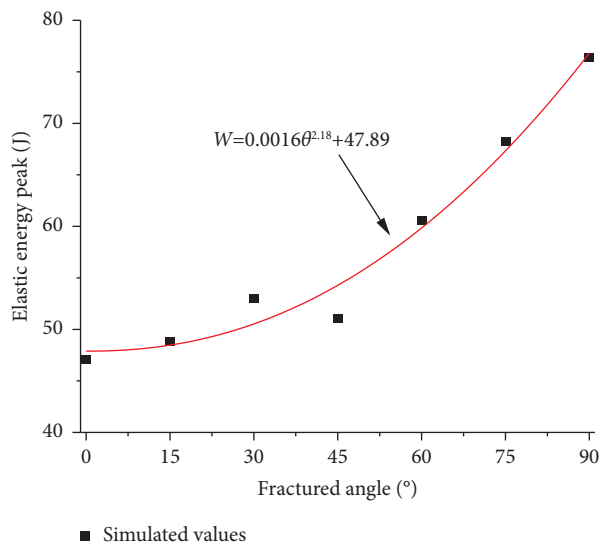

Figure 14: The peak curve of elastic energy at different crack angles.

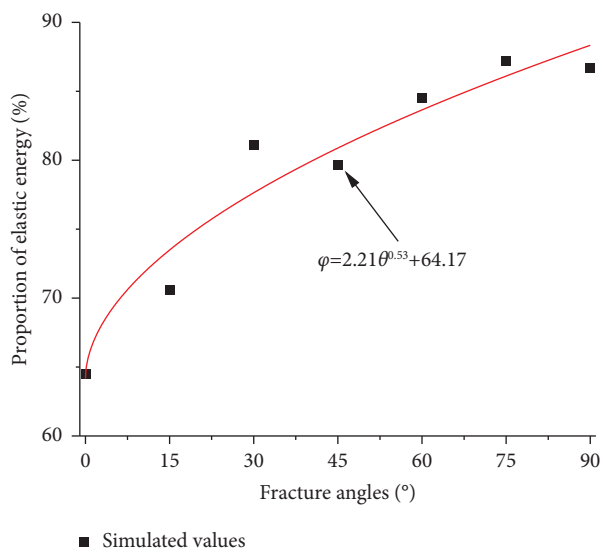

Figure 15: Elastic energy ratio curve at different crack angles.

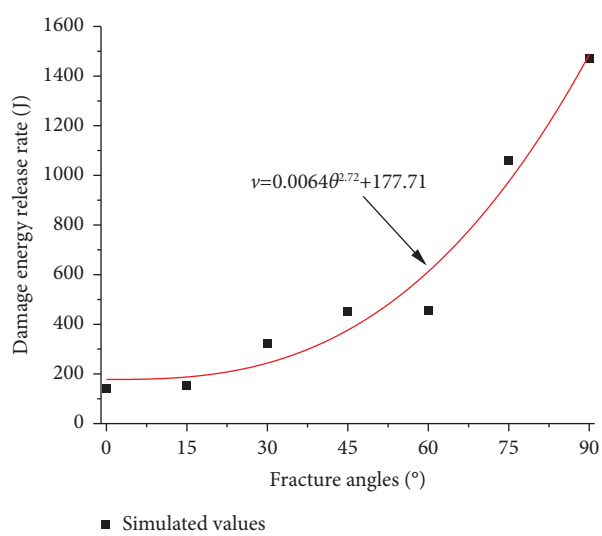

Figure 16: Failure energy release rate curves at different crack angles.

45°, the elastic energy release amount of each 1% strain increases by 215.37%. At 60°, the elastic energy release amount of each 1% strain increases by 217.96%. The elastic energy release per 1% strain at 75° increased by 640.04%, and the elastic energy release per 1% strain at 90° increased by 929.07%. The larger the prefabricated crack angle of the coal body, the elastic energy release amount per 1% strain produced increases in a power function, and the faster the energy release rate is.

4. Conclusions

The indoor test and numerical simulation of coal body under different crack angles were carried out. The burst tendency test of coal body with different crack angles was carried out, and the energy evolution law of coal body under different crack angles was analyzed. The main conclusions are as follows.

Compared with the specimens without prefabricated cracks, the uniaxial compressive strength of the specimens with 0° cracks decreased by 48.4%, the dynamic failure time increased by 279.4%, the burst energy index decreased by 54%, and the burst energy velocity index decreased by 87.9%. After that, with the increase of prefabricated crack angle, the uniaxial compressive strength of coal increases gradually, the dynamic failure time decreases gradually, the burst energy index increases gradually, and the burst energy velocity index increases gradually.

With the increase of prefabricated crack angle, the proportion of elastic energy in front of the peak of coal increases in a power function. The less energy dissipation in the whole loading process of coal, the faster the energy release rate.

The research results can provide some theoretical support for the prevention and control of rock burst disaster.

Data Availability

The data used to support the findings of this study are included within the article.

Conflicts of Interest

The authors declare that they have no conflicts of interest.

Acknowledgments

This research was funded by Shandong Energy Group, grant no. SNKJ2022BJ01-R27.

References

[1] Y. D. Jiang, Y. S. Pan, F. X. Jiang, L. M. Dou, and Y. Ju, "State of the art review on mechanism and prevention of coal bumps in China," *Journal of China Coal Society*, vol. 39, no. 02, pp. 205–213, 2014.

[2] Y. L. Tan, W. Y. Guo, T. B. Zhao, and X. J. Meng, "Coal rib burst mechanism in deep roadway and stress relief-support reinforcement synergetic control and prevention," *Journal of China Coal Society*, vol. 45, no. 01, pp. 66–81, 2020.

[3] P. Shan, W. Li, X. Lai, S. Zhang, X. Chen, and X. Wu, "Research on the response mechanism of coal rock mass under stress and pressure," *Materials*, vol. 16, no. 8, p. 3235, 2023.

[4] Q. Ma, Y. L. Tan, X. S. Liu, Q. H. Gu, and X. B. Li, "Effect of coal thicknesses on energy evolution characteristics of roof rock-coal-floor rock sandwich composite structure and its damage constitutive model," *Composites Part B: Engineering*, vol. 198, Article ID 108086, 2020.

[5] C. Y. Jiang, L. G. Wang, K. Ding, S. Wang, B. Ren, and J. X. Guo, "Experimental study on mechanical and damage evolution characteristics of coal during true triaxial cyclic loading and unloading," *Materials*, vol. 16, no. 6, p. 2384, 2023.

[6] T. B. Zhao, W. Y. Guo, Y. L. Tan, Y. C. Yin, L. S. Cai, and J. F. Pan, "Case studies of rock bursts under complicated geological conditions during multi-seam mining at a depth of 800 m," *Rock Mechanics and Rock Engineering*, vol. 51, no. 5, pp. 1539–1564, 2018.

[7] C. Pang, Y. Shi, X. Wang, B. Li, and H. Luan, "Study on a high-efficiency mining technology system for gas outburst in coal seams-example of an H coal mine," *Minerals*, vol. 12, no. 7, p. 795, 2022.

[8] Q. Ma, X. L. Liu, Y. L. Tan et al., "Numerical study of mechanical properties and microcrack evolution of double-layer composite rock specimens with fissures under uniaxial compression," *Engineering Fracture Mechanics*, vol. 289, Article ID 109403, 2023.

[9] R. Mao, K. Fang, T. B. Zhao, and N. W. Liu, "Failure mechanism of rock with pre-existing surface crack under cone penetration test," *Chinese Journal of Rock Mechanics and Engineering*, vol. 41, no. 06, pp. 1183–1192, 2022.

[10] Y. C. Yin, W. W. Zheng, X. X. Tang, M. L. Xing, Y. B. Zhang, and Y. H. Zhu, "Test study on failure and energy supply characteristics of rock under different loading stiffness," *Engineering Failure Analysis*, vol. 142, Article ID 106796, 2022.

[11] Y. C. Yin, B. Chen, Y. B. Zhang, S. D. He, C. R. Yao, and C. C. Liu, "Experimental study and evaluation on the weakening of bursting liability of coal with boreholes," *Engineering Failure Analysis*, vol. 155, Article ID 107754, 2024.

[12] T. W. Shi, Y. S. Pan, A. W. Wang, and L. P. Dai, "Classification of rock burst in coal mine based on energy storage and release bodies," *Journal of China Coal Society*, vol. 45, no. 02, pp. 524–532, 2020.

[13] Z. Q. Wang, X. F. Gong, and X. B. Gu, "Mechanical properties and energy evolution law of fractured coal under low confining pressure," *Applied Sciences*, vol. 12, no. 23, Article ID 12422, 2022.

[14] Y. Chen, Z. Zhang, C. Cao et al., "Experimental study of mechanical properties and failure characteristics of coal–rock-like composite based on 3D printing technology," *Materials*, vol. 16, no. 10, p. 3681, 2023.

[15] W. Zhang, B. L. Zhang, and T. B. Zhao, "Study on the law of failure acoustic–thermal signal of weakly cemented fractured rock with different dip angles," *Rock Mechanics and Rock Engineering*, vol. 56, no. 6, pp. 4557–4568, 2023.

[16] M. J. Jiang, N. Zhang, Z. F. Shen, and H. Chen, "DEM analyses of crack propagation in flawed rock mass under uniaxial compression," *Rock and Soil Mechanics*, vol. 36, no. 11, pp. 3293–3300+3314, 2015.

[17] H. R. Hu, Y. Y. Lu, B. W. Xia, Y. Luo, J. Peng, and Y. Li, "Damage characteristics of sandstone with different crack angles subjected to true triaxial cyclic loading and unloading,"

Theoretical and Applied Fracture Mechanics, vol. 121, Article ID 103444, 2022.

[18] H. R. Hu, B. W. Xia, Y. Li, Y. Luo, and J. Peng, "Analysis of damage characteristics of fine and medium-fine cracked sandstones under a complex stress path," *Energy Science and Engineering*, vol. 10, no. 9, pp. 3443–3458, 2022.

[19] H. R. Hu, B. W. Xia, Y. F. Luo, and J. Peng, "Energy characteristics of sandstones with different crack angles under true triaxial cyclic loading and unloading," *Energy Science and Engineering*, vol. 10, no. 4, pp. 1418–1430, 2022.

[20] X. S. Liu, Y. L. Tan, J. G. Ning, Y. W. Lu, and Q. H. Gu, "Mechanical properties and damage constitutive model of coal in coal-rock combined body," *International Journal of Rock Mechanics and Mining Sciences*, vol. 110, pp. 140–150, 2018.

[21] W. Zhang, M. L. Xing, and W. Y. Guo, "Study on fracture characteristics of anchored sandstone with precast crack based on double K criterion," *International Journal of Solids and Structures*, vol. 275, Article ID 112296, 2023.

[22] Q. F. Guo, X. Wu, M. F. Cai, F. H. Ren, and J. L. Pan, "Crack initiation mechanism of pre-existing cracked granite," *Journal of China Coal Society*, vol. 44, no. S2, pp. 476–483, 2019.

[23] Y. L. Wang, J. X. Tang, Z. Y. Dai, T. Yi, and X. Y. Li, "Effect of fracture number and aperture on mechanical properties and failure modes of low-strength rock mass," *Journal of China Coal Society*, vol. 43, no. 12, pp. 3338–3347, 2018.

[24] X. Y. Ma, Z. Y. Fu, Y. R. Li, P. F. Zhang, Y. Q. Zhao, and G. P. Ma, "Study on surface subsidence characteristics based on three-dimensional test device for simulating rock strata and surface movement," *Energies*, vol. 15, no. 5, p. 1927, 2022.

[25] W. Zhang, T. B. Zhao, and X. T. Zhang, "Stability analysis and deformation control method of swelling soft rock roadway adjacent to chambers," *Geomechanics and Geophysics for Geo-Energy and Geo-Resources*, vol. 9, no. 1, p. 91, 2023.

[26] Z. H. Wang, W. C. Sun, Y. T. Shui, and H. Gong, "Surface deformation field and fracture propagation mechanism of rock-like samples with pre-existing fracture," *Coal Science and Technology*, 2022.

[27] C. Fuqi, L. Zhonghui, L. Guoai et al., "Influence of prefabricated fissure angle on sandstone damage and infrared radiation temperature characteristics," *Journal of Geophysics and Engineering*, vol. 15, no. 4, pp. 1187–1196, 2018.

[28] X. L. Chi, K. Yang, and Z. Wei, "Investigation of energy and damage evolutions in rock specimens with large-scale inclined prefabricated cracks by uniaxial compression test and ae monitoring," *Advances in Civil Engineering*, vol. 2020, Article ID 8887543, 12 pages, 2020.

[29] F. Q. Gong, Y. J. Zhao, Y. L. Wang, and K. Peng, "Research progress of coal bursting liability indices and coal burst "Human-Coal-Environment" three elements mechanism," *Journal of China Coal Society*, vol. 47, no. 05, pp. 1974–2010, 2022.

[30] Y. S. Pan, L. Geng, and Z. H. Li, "Research on evaluation indices for impact tendency and danger of coal seam," *Journal of China Coal Society*, vol. 35, no. 12, pp. 1975–1978, 2010.

[31] G. Y. Zhao, B. Dai, and C. Ma, "Study of effect of micro-parameters on macroproperties for parallel bonded model," *Chinese Journal of Rock Mechanics and Engineering*, vol. 31, no. 7, pp. 1491–1498, 2012.